

Enhancing Shear Resistance of Dune Sand with Perforated Geotextile Reinforcement

Goudjil Ishak^{(1,2)*}, Kebaili Mustapha⁽²⁾, Talbi Mohammed Abdallah^(1,2), Fetimi Sara⁽²⁾, Mamanou Rayan⁽²⁾, Zermani Messaoud⁽³⁾

¹Laboratory of Exploitation and Valorisation of Natural Resources in Arid Zones (EVRNZA), University Kasdi Merbah of Ouargla, Ouargla, 30000, Algeria

²Department of Civil Engineering and Hydraulics, University Kasdi Merbah of Ouargla, Ouargla, 30000, Algeria.

³AFITEX ALGÉRIE Society, Bordj El Kifan, Algiers, 16031, Algeria.

Corresponding author*: PhD student. GOUDJIL Ishak

E-mail:goudjil.ishak@univ-ouargla.dz;

University KasdiMerbah of Ouargla, Ghardaia Road, BP.511, 30000, Algeria

Phone: +213 674 954 193

Received :13-07-2023

Accepted :12-01-2024

Published : 31-01-2024

Authors' contribution: All authors contributed to the study conception and design. Conceptualization, Methodology, Validation, Formal analysis, Investigation, Supervision, Project administration: [GOUDJIL Ishak] and [KEBAILI Mustapha]; Material preparation, data collection and analysis: [TALBI Mohammed Abdallah]; First Draft: [FETIMI Sara] and [MAMANOU Rayan];Resources: [ZERMANI Messaoud]. All authors read and approved the final manuscript.

Abstract: The study evaluates the shear resistance gain of dune sands reinforced by a geotextile. The reinforcing geotextile is regularly perforated and inserted to provide a fictitious 'cohesion' to the latter. The shear resistance test of the sand, before and after geotextile addition, is perceived through parameterised triaxial tests.

The results showed a gain in 'cohesion' of the sand-geotextile compound up to 380 kPa. However, the internal friction weakens by 16% compared to the sand alone. The optimal pattern of the perforated geotextile has also been identified based on the required shear strength characteristics. The optimisation of the perforation pattern of the geotextile introduced into the sand makes it possible to reduce the surface area of the geotextile used by almost half.

Moreover, the analytical examination of the obtained results makes it possible to predict the values of the 'cohesion' and the friction of the sand-geotextile compound according to the sand used and the chosen pattern of the perforated geotextile. The correlation between experimental results and predicted values exceeds 98%.

Keywords: Dune sand; Shear strength; Geotextile; Perforation; Reinforcement; Entanglement Correlation.

Tob Regul Sci.™ 2024;10(1): 351 - 364

DOI: doi.org/10.18001/TRS.10.1.24

1. Introduction

Dune sand (DS), recognised as an eolian deposit, is a vast tract of natural material found in various regions around the world. In the northern Sahara, this material occupies an area of almost 9 million km², of which approximately 22% is located in Algeria [1–2]. The abundance and gratuity of this material evoke the temptation of its use in civil engineering and linear structures such as roads, railways, agricultural tracks, and trench bottoms [3–4]. The mechanical advantages of this dune sand are indisputable and noticeably appreciated compared with finer materials such as silts and clays [5–7]. These advantages include permeability, bearing capacity, friction, resistance to compaction, abrasion, wear, dissolution/solubility, and chemical aggression [8–11]. In addition, dune sand has typical advantages over other types of sand, such as alluvial, crushing, and carbonate. Among its advantages is that it is available in large quantities, concentrated in multiple zones, and already sorted by size into solid grains. In addition, it is easy to extract and contains a high proportion of insoluble particles, making it resistant to water and chemical agents. In contrast, some intrinsic defects are recognised as typical characteristics of dune sand (DS). These include friability, brittle behaviour, slope instability, collapse of excavations, and often rather loose conditions [12–15]. A long-targeted objective of the scientific and technical community is the development of DS [16–23]. That is to say, to benefit from its physical and mechanical advantages in parallel with compensation for its defects via various technical tricks. Dune sands are widespread in the northern Sahara but are almost unused in several technical fields such as civil engineering, geotechnical works, agriculture, industry, crafts, and tourism. Several studies have investigated the effect of geotextile (GTX) reinforcement on the shear strength of sandy soil. Denine et al. [2–26] highlighted the positive impact of geotextile reinforcement on the mechanical behaviour of loose sand. Studies have shown that geotextile inclusion increases shear strength and cohesion (C) value, with higher confining pressure restricting sand shear dilatancy and reinforcing effect. Benessalah et al. [26] and Abdelkader et al. [27] also investigated the impact of geotextiles on stress-strain and volumetric change behaviour in reinforced sandy soil, with both studies showing an increase in stress deviator and volume contraction. Feng et al. [28] revealed that geotextiles significantly reinforce desert sand, with geogrid-nonwoven composites showing the highest strength and ductility. Similarly, Skuodis et al. [29] found that reinforced sand samples exhibit higher shearing strength than unreinforced samples. Reza Jamshidi Chenari et al. [30] investigated the interface properties between sand-expanded polystyrene mixtures and geogrid reinforcement under cyclic loading. Experiments show that adding 0.9% EPS beads to the sand bed decreases interface shear stiffness by 30% to 63%, while interface damping increases twice. The hardening factor also increases with cycle number under different stress levels. This study is crucial for designing geosynthetic-reinforced soil structures. Markou [32–33] investigated the impact of sand grain shape and size on the mechanical behaviour of geotextile-reinforced sands. Both studies demonstrated that reinforced sands exhibit higher strength and axial strain at failure. Lakkimsetti and Latha [33] also highlighted the positive impact of geotextile inclusion on sand resistance to liquefaction. They observed that geotextile inclusion increased liquefaction resistance and post-liquefaction shear strength, especially for angular particles. Lal et al. [34] studied the behaviour of coir geotextile-reinforced sandy soil foundations and showed that coir geocell reinforcement offers superior performance compared with planar and discrete forms. Goodarzi and Shahnazari [35] examined the mechanical behaviour of carbonate sand reinforced with horizontal geotextile layers using drained compression triaxial tests. Their results reveal that geotextile inclusion increases peak strength and strain at failure while reducing post-peak strength loss. Strength enhancement is greater at high strains, and increased relative density increases peak strength. Hussein Aldeeky et al. [36] They examined the impact of sand placement method on interface shear strength behaviour in geotextile layers. Seven types of woven and non-woven geotextiles were used with poorly graded sand. They found that deposit plane significantly influenced soil behaviour, particularly for non-woven geotextiles. Higher mass per unit area and opening sizes resulted in higher interface friction angles.

This study is based on the same technology and benefits geotechnical engineering by combining DS with a geotextile (GTX) to overcome rheological issues. The new material investigated in this research is a mix of dune sand and perforated geotextile (DS/GTX). Some mechanical quantities of this compound were measured and compared

with those of commonly used materials to identify potential variables and assess the likelihood of using the compound in question in the appropriate domains. Another objective of this study is to indirectly estimate the shear strength characteristics of the DS/GTX compound based on the physical parameters of the two materials (DS and GTX). The results of this study are not sufficient to determine whether the DS/GTX compound is suitable for road construction. However, it does shed light on the importance of local material recovery. The motivation behind this research stems from the extensive potential for the profitable use of DS. This resource is abundant, cost-effective, and easily modifiable; however, its application remains largely untapped.

This study aims to measure and investigate the shear strength of a DS/GTX compound while considering the geometric configuration of the GTX integrated with sand. GTX layers were placed on the sand matrix to improve cohesion in the DS. The GTX is regularly perforated to promote its entanglement with sand and to economise the amount of GTX material used. The perforation pattern of GTX was varied to observe its influence on the shear strength parameters of the DS/GTX compound.

2. Analytical Approach

The analytical approach adopted in this study is mainly experimental. It consists of performing triaxial tests of the drained consolidated type (CD), on sand alone (DS), and then on the DS/GTX compound. A GTX disc was placed in the middle of the sand specimen (Figure 1). The compound, thus prepared, was submitted to the usual triaxial test (CD). The GTX has perforated according to a rectangular grid, in which the diameter (ϕ) of the holes and the spacing (SP) between them changed for each test performed.

The triaxial shear tests follow a standard experimental procedure. The shear strength properties of sand alone (DS) and when combined with GTX (DS/GTX) are determined by analysing stress results plotted on the Mohr-Coulomb plane. These characteristics are usually known (cohesion and internal friction angle). For the specific case of the DS/GTX compound, the cohesion deduced from the tests performed is noted as 'cohesion' in quotation marks to remind us that, in reality, it is fictitious compared to the DS and due only to the GTX introduced in the sand matrix.

Taking into account that the results of this experimental investigation will be projected on a road project located in the region of Ouargla in the South-East of Algeria (Latitude: 31.9629, Longitude: 5.34193, Altitude: 123m to 315m), the sand specimens tested must be formed in a dry state. This aims to simulate the arid (dry) conditions of the region where these road projects are carried out. To prepare specimens for triaxial tests, follow these simple steps:

- Filling the cylindrical mould ($\phi=5\text{cm}$ and $H=10\text{cm}$) with sand up to mid-height, then vibration,
- Placement of the GTX sheet prepared in the form of a circular disc and regularly perforated (Figure 2),
- Filling the cylindrical mould with vibration until it reaches its total height ($H=10\text{cm}$)

At the end of this preparation, all the specimens are obtained from almost the same density of the material to be tested (1.75 ± 0.1). In addition, the CD indication of the tests performed does not insinuate the presence of water in the prepared DS/GTX compound. The total stresses (σ_3 and σ_1) applied to the specimens are themselves the actual stresses ($\sigma'_3 = \sigma_3$ and $\sigma'_1 = \sigma_1$). No water or water pressure exists.

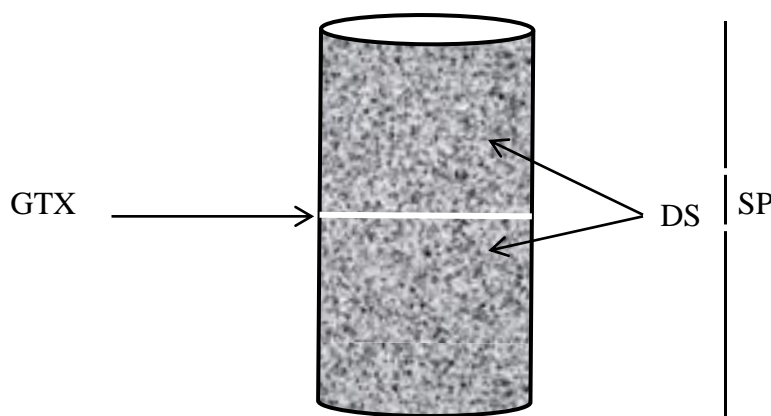


Figure 1: Location of the GTX in the sand specimen

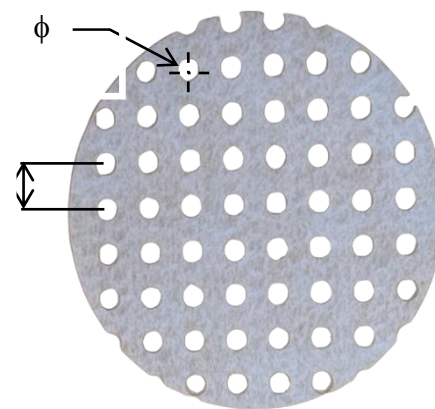


Figure 2: The GTX perforating pattern

Table 1 expresses the characteristics of the two materials used: dune sand and geotextile. Figure 3 shows the particle size distribution of the dune sand used. The two materials shown in Table 1 and Figure 3 have the following physical and mechanical characteristics:

Table 1: Characteristics of the used materials (DS) and (GTX).

Dune sand (DS)		Geotextile (GTX)	
Sampling site	Sidi Khouiled	Nomination	AS10
Grain Density (kN/m ³)	27.1	Area Density (g/m ²)	100
Minimum Density (kN/m ³)	13.4	Thickness below 2 kPa (mm)	0.5
Maximum Density (kN/m ³)	17.7	Tensile strength(kN/m)	MD* 6
Natural Density (kN/m ³)	17.2		CMD* 7
Sand equivalent (%)	76.62	Maximum tensile strain (%)	MD* 70
Porosity (%)	18.25		CMD* 90
Natural water content (%)	2.5	Dynamic perforation (mm)	30
uniformity coefficient	1.74	Resistance to CBR punching (kN)	1
Curvature coefficient	0.89	Resistance to pyramidal punching (kN)	0.7
Internal friction angle (°)	33.35	Normal permeability on the plan (m/sec)	0.08
Cohesion (kPa)	0	Filtration opening (μm)	90

MD* Machine direction (Longitudinal) CMD* Cross-machine direction (Transversal)

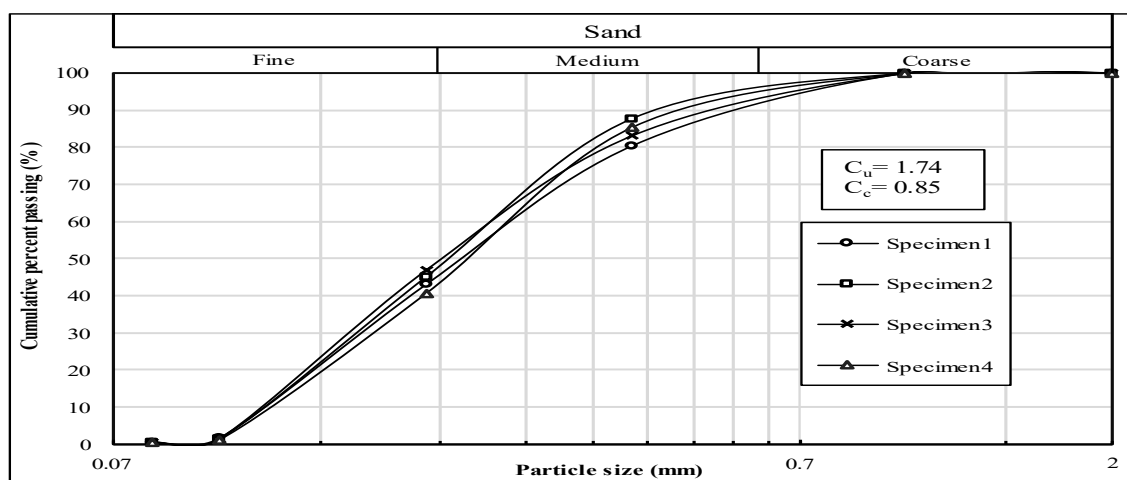


Figure 3: Particle size curves of the dune sand used (MIT classification)

- The dune sand (DS) used is of fairly tight particle size and contains very few fines and impurities. This is a direct consequence of how this sand formed. Local wind intensity must have selected the solid grains of sand deposited in the study area. The size of the grains of sand stands out as a very observable characteristic of this material. Moreover, the modest difference between the natural density of the sand and its dense mass attests to a low compaction capacity. In other words, the sand piles up almost wholly by simple deposition in place. Its tight grain size gives it quite more compaction. In addition, the sand is relatively porous, even permeable. Its internal friction is also well appreciated. Its loose state becomes apparent because of the zero value of its cohesion.
- Geotextile does not have specific characteristics except that it gets chosen from those of low quality. This is to limit (up to the threshold of required technical performance) the cost of the DS/GTX compound. The weak physical characteristics of the GTX are observable due to its surface mass and thickness. Its various resistances are substantial and testify to a low mechanical quality.

The dimensions of the cylindrical sandy specimen are $\phi_{ep}=5\text{cm}$ and $H_{ep}=10\text{cm}$. Among the concepts demonstrated in shear rupture mechanics is the failure plane of a shear-stress material inclined from the horizontal [37]:

$$\theta = \frac{\pi}{4} + \frac{\varphi''}{2} \quad (1)$$

Where φ'' means the internal friction angle of the material in question. For the compound case (DS/GTX), this plane must encounter the GTX layer placed at the mid-height of the test specimen (Figure 4). Considering the combined composition of the compound (DS/GTX), the angle (φ''), shown here, is between:

- The internal friction angle of sand alone: $\varphi_{DS} = 33.35^\circ$ (Table 1), and
- The friction angle of the DS/GTX compound: $19.29^\circ < \varphi < 29.03^\circ$ (Section 3: figure 7).

Therefore, $19.29^\circ < \varphi'' < 33.35^\circ$, which makes $54.65^\circ < \theta < 59.52^\circ$. The included GTX in the sand intercepts the failure plane by triaxial shear (Figure 4).

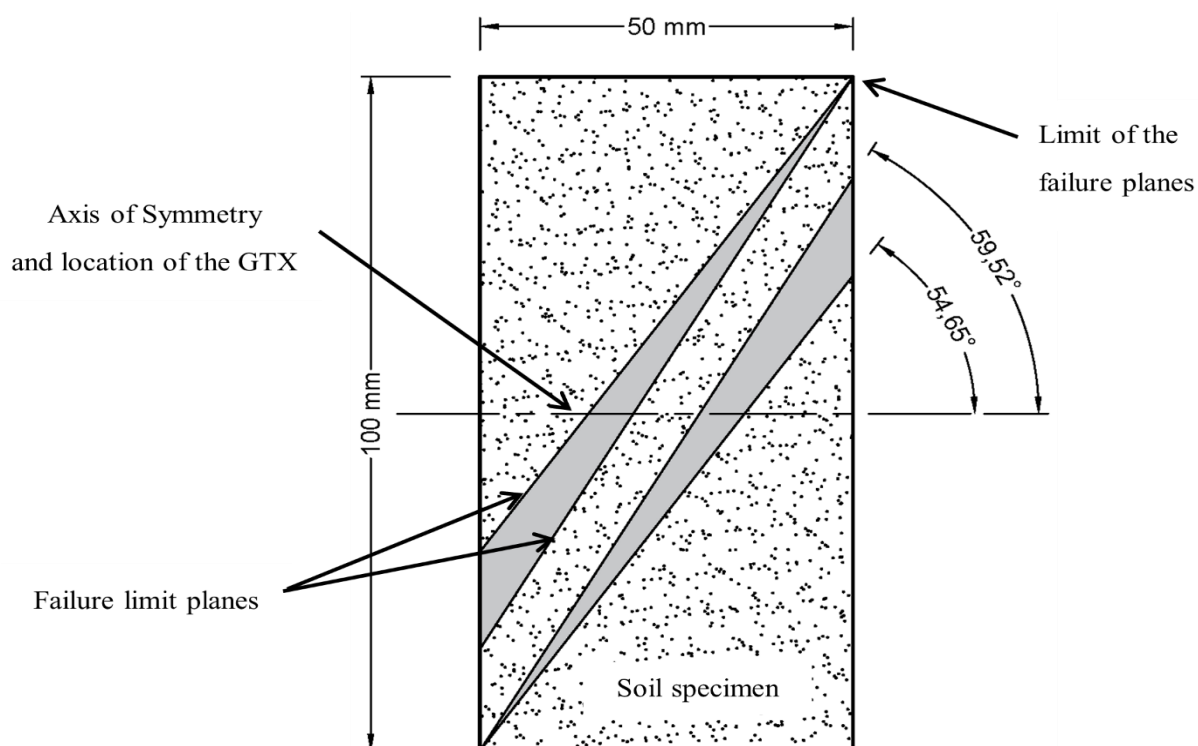


Figure 4: Range of the triaxial failure plane.

3. Results And Interpretations

Figure 5 shows the variation of the deviatoric stress ($\Delta\sigma$) versus a function of the axial deformation of the sand specimens alone (DS). Figure 6 is an example (among the results obtained) of variation of the same dimension ($\Delta\sigma$) for the case of sand reinforced by GTX. Both families of curves show an inclined behaviour leaning towards a not-very-fragile rupture. The membrane presence around the test specimens must have masked the peak generally seen on the compression curve of the sand alone.

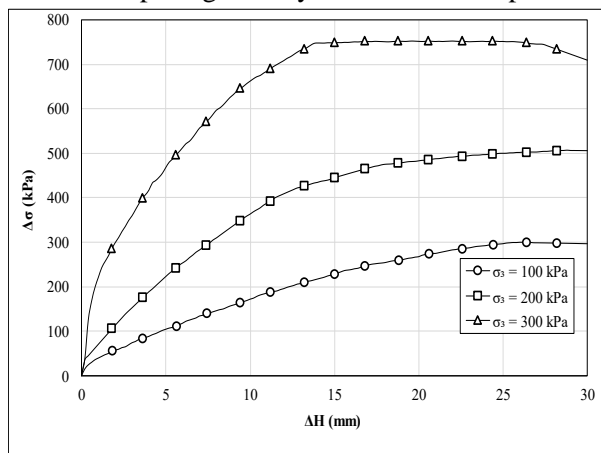


Figure 5: $\Delta\sigma(\Delta H)$, case of sand alone.

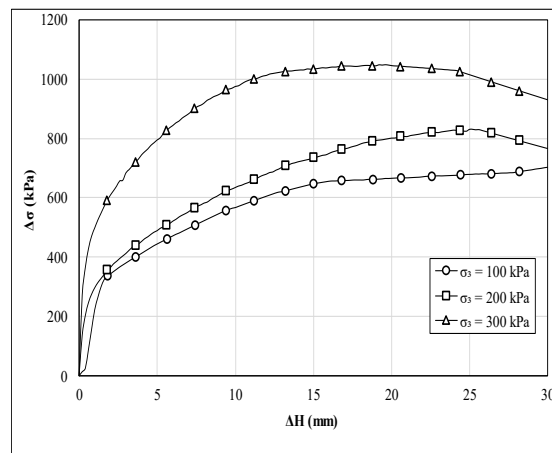


Figure 6: $\Delta\sigma(\Delta H)$, case of sand+ GTX (4-7).

Table 2 displays first the percentage of perforated GTX material compared to the unperforated unit area. This percentage is, obviously, all the more reduced as the perforations are large and closely spaced. In the case of perforations 8-11, where $\phi=8\text{mm}$ and $\text{SP}=11\text{mm}$, the gain of GTX material is almost half.

Table 2 also shows the values of the maximum deviatoric stress recorded (respectively) in each test. These are the values assigned to the rupture of the tested specimens. Table 2 clearly shows an increase in the deviatoric stress with the spacing between the holes of the perforated GTX. This finding is valid:

- both the diameters (4mm and 8mm) suggest that this variation is independent of the perforation diameter.
- for each confining stress case $\sigma_3= 100\text{kPa}$, $\sigma_3= 200\text{kPa}$ et $\sigma_3= 300\text{kPa}$. Therefore, this result can be projected on the axial stress (i.e. major principal stress) as long as the latter is only the sum ($\sigma_3 + \Delta\sigma$).

Table 2: Deviatoric stresses ($\Delta\sigma_{\text{Max}}$) recorded at failure

		GTX area (%)	$\Delta\sigma_{\text{Max}}$ (kPa)		
			$\sigma_3= 100\text{ kPa}$	$\sigma_3= 200\text{ kPa}$	$\sigma_3= 300\text{ kPa}$
Dune Sand alone		0.00	299	507	753
DS/GTX $\phi(\text{mm})\text{-SP}(\text{mm})$	4-7	74.35	702	831	1048
	4-9	84.49	851	913	1117
	4-11	89.61	991	1120	1184

4-13	92.56	1091	1099	1292
8-11	58.46	718	1004	1187
8-13	70.26	900	1029	1215
8-15	77.66	1100	1245	1287
8-17	82.61	1161	1174	1372

Table 2 additionally presents a decrease in the deviatoric stress (σ_3) with the diameter (ϕ) of the perforations. The comparative values of (σ_3) between (respectively) the pairs of patterns (4-11 and 8-11) and (4-13 and 8-13) attest to this decrease. This influence of the diameter of the perforations is logical because the larger the diameter, the more one tends to an unreinforced sand. That means low resistance to the deviatoric stress (σ_3) or that axial (σ_1).

After conducting shear tests often, Mohr circles of stresses were created for the harmonic values of 3 and 1, which helped determine the shear strength parameters (C and ϕ). Figures 7 and 8 summarise all the results obtained for the shear strength characteristics (C and ϕ). The curves shown in Figure 7 represent:

- the variation in cohesion according to the spacing between the perforations (diameter 4mm and 8mm),
- the variation in friction angle according to the spacing between the perforations (diameter 4mm and 8mm),
- The cohesion and friction angle values of dune sand reinforced with unperforated GTX have been successfully obtained and analysed.

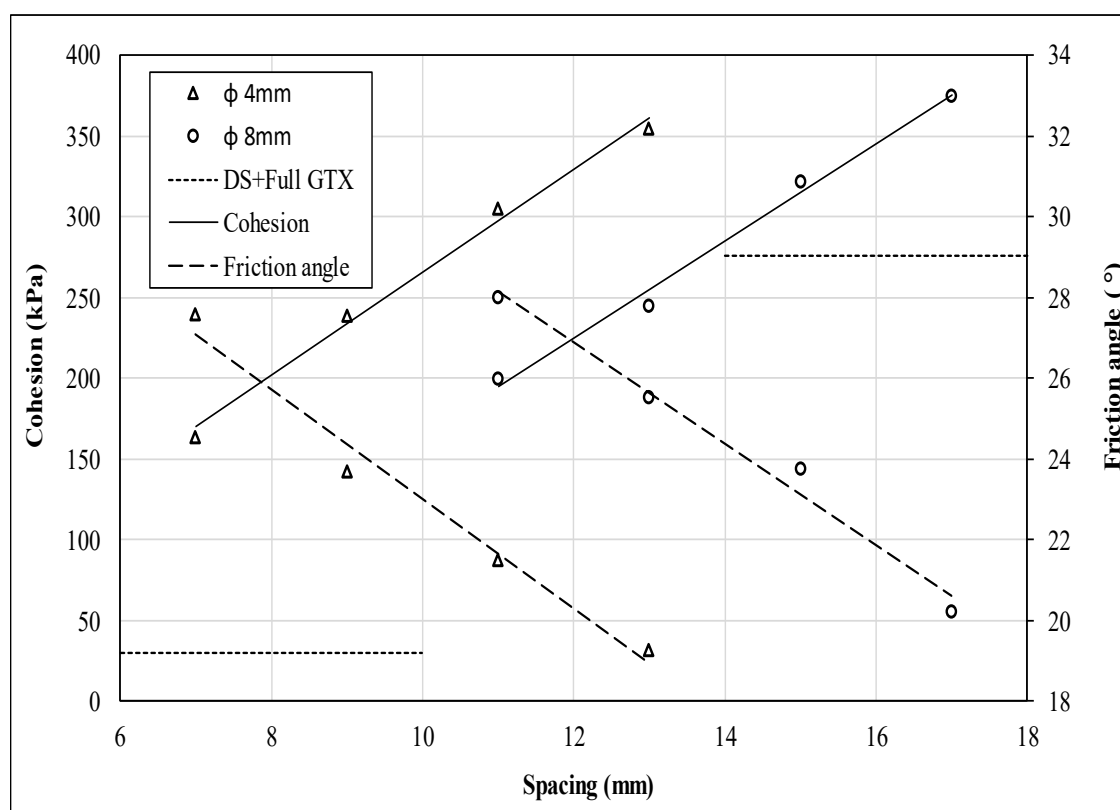


Figure 7: Shear strength characteristics of DS/GTX material as a function of ϕ and SP.

The results shown in Figure 7 demonstrate a nearly linear change in both cohesion and friction angle of the DS/GTX combination with variations in the distance between perforations. Cohesion (C), even if considered fictitious, within the DS/GTX compound increases when the spacing between the perforations increases. In contrast, the compound friction angle (ϕ) decreases when the spacing between the perforations increases. These two observations apply to both diameters of the perforations (4mm and 8mm).

The representative curves of the friction angle (Figure 7) show that the latter is even closer to that of sand alone ($\phi = 33.35^\circ$) because the spacing (SP) between the perforations is small. This is a logical and consistent outcome, and the same applies to the case of 'cohesion'. As the distance between the holes decreases, cohesion tends to decrease as well, with the lowest values reached at the limit of sand alone ($C = 0 \text{ kPa}$). These variations can be accounted for by the fact that:

- when the perforations are close to each other (so SP is small), there is little GTX at the crossing of the fracture plane of the specimens tested in the triaxial test. The less GTX there is in the compound material, the sandier it is and, therefore, of sandy characteristics (C and ϕ).
- In contrast, since the DS-GTX friction is lower than the internal friction of the DS (29.03° compared to 33.35°), it becomes understandable that the more SP increases, the larger the GTX surface included in the DS makes the friction tend toward values increasingly close to that of DS-GTX. That is to say, down.
- as well as the reasoning adopted for the friction between the two materials (DS and GTX), the 'cohesion' between the two materials is undeniable given the adhesion of the grains of sand on the surface of the GTX and also the 'cohesion' detected through the shear tests carried out. A 'cohesion' gain is noted (30 kPa between sand and the entire GTX, compared to 0 kPa for DS alone). It becomes understandable that the more SP increases, the larger the area of GTX included in the DS, which increases the 'cohesion' and makes it tend towards that between sand and the entire GTX.

Finally, Figure 7 clearly shows a reproduction of the curve shapes representative of the diameter of the 8mm holes compared to those representative of the 4mm diameter. The extreme results of the two characteristics (C and ϕ) are recognized, sweeping a broad spectrum of values manipulated in practice: $164 \text{ kPa} \leq C \leq 375 \text{ kPa}$ and $19.29^\circ \leq \phi \leq 28.03^\circ$. Values slightly exceeding these limits are desired using simple extrapolation based on the available linear lines. Reducing the SP spaces may result in the overlapping of perforations, leading to the loss of the perforation network's regular structure. Similarly, a tendency to extrapolate the lines representative of the results obtained does not seem necessary as long as the 'cohesion' reached is already appreciable enough (375 kPa).

The combinations (ϕ -SP) giving a minimum of GTX material used per unit area of it are the (4-7) and the (8-11). Based on Table 2, the corresponding percentages of GTX material per unit perforated area are 74.35% and 58.46%, respectively. Referring to Figure 7, the C and ϕ of these two combinations show a slight loss in friction compared to the case of sand alone (28.03° compared to 33.35°), but an enormous gain in cohesion qualified as fictitious: 164 kPa compared to 0 kPa. It is an extraordinary gain that perfectly compensates for the cohesion defect indicated in section 1 (INTRODUCTION) of this article. Keep in mind the saving of almost half of GTX material.

Figure 8 shows the same values of shear strength characteristics (C and ϕ) as a percentage of GTX available after perforation via any pattern (ϕ , SP). As shown in Figure 7, cohesion increases, and friction decreases as the spacing between perforations increases, i.e., the available percentage area of the perforated GTX ($GTX_{\text{available}}$) tends to be 100%. This remains valid up to ($GTX_{\text{available}}$) almost 100% (figure 8). When ($GTX_{\text{available}}$) approaches 100%, a change inversion is observed. This is explained by the fact that when ($GTX_{\text{available}}$) is almost 100%, i.e., the perforation pattern has nearly disappeared, it is the pattern and manufacturing method of the GTX that controls the shear resistance at the DS-GTX interface. The manufacturing method of the GTX includes all the descriptive aspects such as woven, non-woven: needled, thermo-linked, or knitted. On a scale of less than a millimetre, such aspects are

manifested in terms of the GTX surface roughness, the porosities and the spaces between the constituent filaments. So, the texture of the GTX is expressed as (C) and (φ) rather than the perforation pattern itself.

This resonance and interpretation are supported by the proximity of the curves associated with $\phi=4\text{mm}$ of the 100% limit compared to those associated with $\phi=8\text{mm}$ (Figure 8). In other words, when the perforation diameter of the GTX approaches the size of the gaps and pores specific to the texture of the manufactured GTX.

Moreover, Figure 8 expresses a preferential order of perforation pattern concerning the economy in GTX material used. The distinction between the curves relating to $\phi=4\text{mm}$ and that for $\phi=8\text{mm}$ results in the same percentage of GTX surface available after perforation ($\text{GTX}_{\text{available}}$):

- if the cohesion, even if apparent, of the DS/GTX compound is claimed, the preferred perforation diameter should be large (8mm for the case of this research).
- if, on the contrary, it is the friction that is stressed, the diameter of the perforation should be small (4mm for the case of the present investigation).

The above two deductions are valid, as shown in Figure 8, up to an $\text{GTX}_{\text{available}}$ limit of about 80%. When this rate exceeds this limit, the texture effects of the GTX come into line and significantly affect the expression of shear strength on the DS-GTX interface.

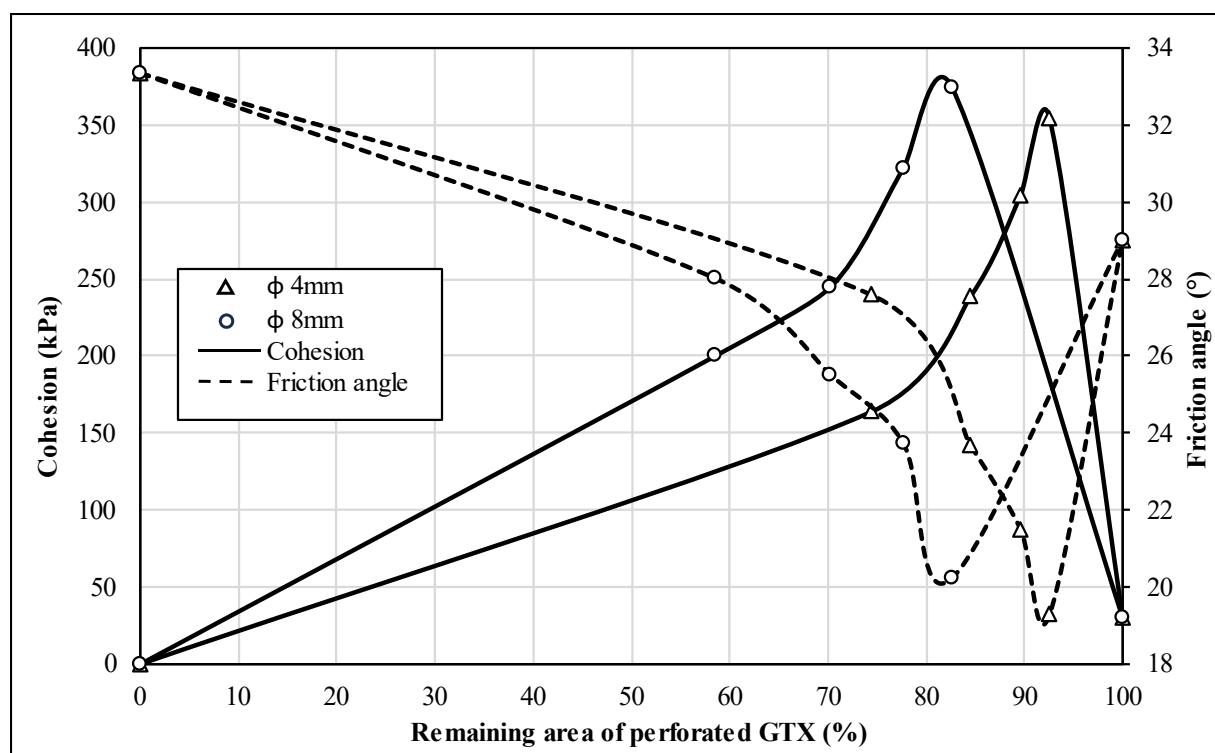


Figure 8: Variation of the shear strength parameters of the compound (DS/GTX) according to the available surface of the perforated GTX.

4. Analytical Treatment

In view of the almost straight lines results obtained (Figure 7), the observed linear variations can be analytically expressed. Table 3 groups the linear equations from the results obtained for cohesion (C) and friction angle (φ) shown in Figure 7.

Table 3: Analytical equations for C and ϕ , and corresponding correlation coefficients.

		DS alone	DS/GTX ($\phi=4$ mm)	DS/GTX ($\phi=8$ mm)	DS+ Full GTX
Cohesion (kPa)	Equation	C = 0	C = 31.95 SP - 53.75	C = 30.1 SP - 135.9	C = 30.01
	Correlation coefficient		99.23 (%)	99.06 (%)	
Friction Angle ($^{\circ}$)	Equation	$\phi = 33.35$	$\phi = 36.58 - 1.356$ SP	$\phi = 41.983 - 1.257$ SP	$\phi = 29.03$
	Correlation coefficient		97.68 (%)	98.27 (%)	

The almost straight lines of the variations in Figure 7 show that the slope of the curves (C-SP and ϕ -SP, respectively) are independent:

- The perforation diameter of the GTX: it is the same slope whether it is the diameter $\phi=4$ mm or $\phi=8$ mm,
- The spacing between perforations is due to the consistency of the slope over the entire SP interval.

The variation of the perforation pattern of the GTX (ϕ and SP), thus, does not affect the values of the observed slopes. It can, therefore, be assumed that the type of sand used significantly affects the slope of the resultant straight lines. C_u is one of the most representative and intrinsic parameters of sand particle size. The uniformity coefficient bias ($C_u=1.74$, as shown in Table 1) is an excellent example of the latter. The starting ordinate of each line (respectively $\phi=4$ mm or $\phi=8$ mm) is visibly proven related to the perforation diameter of the GTX.

For the case of cohesion (C), the two equations obtained at the end of Figure 7 (Table 3) are of the type $C = a.SP + b$ where (a) is very close to the value 31 and (b) variable according to the diameter (ϕ). Linking the values of (b) with those of diameter (ϕ), (-53.75 kPa and -135.9 kPa with, respectively, 4mm and 8mm) resulted in $b = 28.4 - 20.54\phi$.

Similarly, for the case of the internal friction angle (ϕ), the two equations obtained at the end of Figure 7 (Table 3) are of the type $\phi = a'. SP + b'$ where (a') is on average equal to -1.3 and (b') variable according to the diameter (ϕ). Linking the values of (b') with those of the diameter (ϕ), (36.58 $^{\circ}$ and 41.98 $^{\circ}$ with, respectively, 4mm and 8mm) resulted in $b' = 1.35\phi + 31.18$.

Hence, the equations of the 04 lines shown in Figure 7, after the expression of the slopes (a) as a function of the coefficient of uniformity of the sand ($C_u=1.74$):

$$\text{DS/GTX } (\phi = 4 \text{ mm}): C = 18.36 C_u \times SP - 20.54 \phi + 28.4 \text{ and } \phi = 1.35 \phi - 0.78 C_u \times SP + 31.18 \quad (2)$$

$$\text{DS/GTX } (\phi = 8 \text{ mm}): C = 17.30 C_u \times SP - 20.54 \phi + 28.4 \text{ and } \phi = 1.35 \phi - 0.72 C_u \times SP + 31.18 \quad (3)$$

Considering the values very close to the (respective) coefficients shown in the above equations, the latter can simplify to:

$$C(\text{kPa}) = 17.83 C_u \times SP - 20.54 \phi + 28.4 \quad \text{and} \quad \phi(^{\circ}) = 1.35 \phi - 0.75 C_u \times SP + 31.18 \quad (4)$$

Where SP and ϕ are expressed in mm.

These last two empirical relationships allow a prediction of the 'fictitious cohesion' and the internal friction of the DS/GTX compound based on the knowledge of the particle size of the sand used (represented by the uniformity coefficient) and the perforation pattern of the GTX. That is the perforation diameter and the spacing between the perforations. This deduction can be retained at least for the interval of the diameters of the perforations and the spacing manipulated.

5. Conclusion

At the end of the study, some remarkable results are worth recalling. These are, indeed, exploitable on the academic and application levels. The conclusions outlined in this section lead to a technical framework for the valorisation of dune sand, recognized as almost free and abundant in southern Algeria but very little used in several economic sectors.

A low-quality geotextile is voluntarily associated with dune sand to guarantee a low-cost price for the manufactured compound. The association of the perforated geotextile with the sand of dunes demonstrates a notable compensation for the lack of cohesion of the sand. The cohesion of the DS/GTX compound, even if said fictitious because due to geotextile, exceeds 164 kPa, while it is zero for sand alone. The internal friction of the compound is little reduced: 28° compared to 33° for sand alone. The perforation of the GTX promotes the entanglement of the latter with the sand and reduces, up to half, the amount of geotextile material used.

The GTX's perforation patterns are carefully chosen and used as indicators to find the best configuration for the compound material. Through several triaxial tests conducted solely on perforations with diameters of 4mm and 8mm, it has been discovered that the 8mm perforation is ideal for determining the compound's cohesion, while the 4mm perforation is better suited for assessing its friction. When the perforations approach the millimetre scale, the effect of the GTX texture becomes sensitive and affects the measurement results targeted for the applied perforation pattern.

In addition, the analytical treatment of the results of the shear strength characteristics of the DS/GTX compound allowed us to deduce two empirical expressions. These permit us to predict, quite absolutely (likelihood exceeding 97%), the 'cohesion' of the DS/GTX compound and its internal friction according to the grain size of the sand used and the perforation pattern of the geotextile used. The demonstrated expressions function as tools for estimating the shear strength parameters of a dune sand and geotextile compound.

6 Recommendations

In conclusion, the study suggested the following recommendations for practical purposes, such as enhancing and expanding upon the ideas explored. These recommendations are closely related to the fundamental concept of this research, which is to exploit dune sand for geotechnical purposes.

- A good complement to the results of the tests carried out lies in the modification (quite numerous) of the perforation pattern (ϕ and SP) of the GTX included in the sand. A selection of the most accurate results, as well as a statistical treatment of the latter, are strongly indicated before attempting their interpretation or inferring a conclusion.
- The study could cover several types of geotextiles, but it is vital to consider their economic feasibility. Furthermore, various types of sand could also be studied, especially if they are easily accessible. The method used to establish a predictive model for the compound's behaviour under shear stress can be replicated in this study. However, it will take many tests and comparisons with direct measurements of shear resistance parameters to develop a predictive model for the cohesion and friction of the sand/geotextile compound.
- The customary analytical systems can incorporate many other physical parameters of sand and geotextile materials. Similarly, the results and deductions should be confronted from various mathematical and practical analyses to reach

the most general conclusions possible. The design of experiments (DOE) methodology strongly indicates investigative techniques to detect key parameters influencing the shear resistance indicators of the compound. These parameters encompass attributes such as perforation shape, dimensions, hole spacing, GTX thickness, and toughness of the latter...Moreover, a numerical simulation of the parameters and quantities concerning the shear resistance of the perforated GTX-reinforced sand must be intriguing to study. However, it requires a large number of tests in order to evaluate the interface effects between sand and the geotextile layer for each perforation pattern. Therefore, a more efficient approach involves relying on tests to evaluate this lift.

Acknowledgement

The authors would like to thank AFITEX-ALGERIE society and recognize the services it has kindly provided for the feasibility purpose of this study.

References

1. Bouallala M, Neffar S, Chenchouni H (2020) Vegetation traits are accurate indicators of how do plants beat the heat in drylands: Diversity and functional traits of vegetation associated with water towers in the Sahara Desert. *Ecol Indic* 114:. <https://doi.org/10.1016/j.ecolind.2020.106364>
2. Miara MD, Teixidor-Toneu I, Sahnoun T, Bendif H, Ait Hammou M (2019) Herbal remedies and traditional knowledge of the Tuareg community in the region of Illizi (Algerian Sahara). *J Arid Environ* 167:65–73. <https://doi.org/10.1016/j.jaridenv.2019.04.020>
3. Hornsey WP, Carley JT, Coghlan IR, Cox RJ (2011) Geotextile sand container shoreline protection systems: Design and application. *Geotextiles and Geomembranes* 29:425–439. <https://doi.org/10.1016/j.geotextmem.2011.01.009>
4. Naeini SA, Gholampoor N (2014) Cyclic behaviour of dry silty sand reinforced with a geotextile. *Geotextiles and Geomembranes* 42:611–619. <https://doi.org/10.1016/j.geotextmem.2014.10.003>
5. Fattah MY, Joni HH, Al-Dulaimy ASA (2018) Strength characteristics of dune sand stabilized with lime-silica fume mix. *International Journal of Pavement Engineering* 19:874–882. <https://doi.org/10.1080/10298436.2016.1215687>
6. Li X, Xu W, Chang L, Yang W (2022) Shear Behaviour of Aeolian Sand with Different Density and Confining Pressure. *Applied Sciences (Switzerland)* 12:. <https://doi.org/10.3390/app12063020>
7. You Q, Yang Z, Ma J, Yan X, Sesay T, Wang H, Liang Z (2022) Analysis of the Particle Characteristics of Aeolian Sand in Yulin Area, China. *Advances in Civil Engineering* 2022:. <https://doi.org/10.1155/2022/7533159>
8. Aflaki E, Hajiannia A (2015) Stabilization of sand dunes with oil residue: Application to civil engineering construction and environmental implications. *J Cent South Univ* 22:3059–3068. <https://doi.org/10.1007/s11771-015-2842-x>
9. Hadjadj K, Chihi S Rietveld Refinement Based Quantitative Phase Analysis (QPA) of Ouargla (Part of Grand Erg Oriental in Algeria) Dunes Sand. <https://doi.org/10.1007/s12633-020-00826-2/Published>
10. Padmakumar GP, Srinivas K, Uday K V., Iyer KR, Pathak P, Keshava SM, Singh DN (2012) Characterization of aeolian sands from Indian desert. *Eng Geol* 139–140:38–49. <https://doi.org/10.1016/j.enggeo.2012.04.005>

11. Smaida A, Haddadi S, Nechnech A (2019) Improvement of the mechanical performance of dune sand for using in flexible pavements. *Constr Build Mater* 208:464–471. <https://doi.org/10.1016/j.conbuildmat.2019.03.041>
12. Fattah MY, Joni HH, Ahmed AS (2016) Compaction and collapse characteristics of dune sand stabilized with lime-silica fume mix. *Turkish Journal of Engineering and Environmental Sciences* 40:99–113. <https://doi.org/10.15446/esrj.v20n2.50724>
13. Shabani K, Bahmani M, Fatehi H, Chang I (2022) Improvement of the geotechnical engineering properties of dune sand using a plant-based biopolymer named serish. *Geomechanics and Engineering* 29:535–548. <https://doi.org/10.12989/gae.2022.29.5.535>
14. Yuan Y, Wang X, Zhou X (2008) Experimental research on compaction characteristics of aeolian sand. *Frontiers of Architecture and Civil Engineering in China* 2:359–365. <https://doi.org/10.1007/s11709-008-0053-3>
15. Siddique SN, Deng J, Mohamedelhassan E (2023) Improving the Strength Properties of Sand Using Laponite, a Promising Nanoparticle. *International Journal of Civil Engineering* 21:679–693. <https://doi.org/10.1007/s40999-022-00791-4>
16. Arias-Trujillo J, Matías-Sánchez A, Cantero B, López-Querol S (2023) Mechanical stabilization of aeolian sand with ceramic brick waste aggregates. *Constr Build Mater* 363:129846. <https://doi.org/https://doi.org/10.1016/j.conbuildmat.2022.129846>
17. Elsayy MBD (2021) PERFORMANCE OF SAND DUNES IN STABILIZING HIGHLY EXPANSIVE SOIL. *Journal of GeoEngineering* 16:23–34. [https://doi.org/10.6310/jog.202103_16\(1\).3](https://doi.org/10.6310/jog.202103_16(1).3)
18. Gao B, Liu X, Liu J, Song L, Shi Y, Yang Y (2023) Field Characterization of Dynamic Response of Geocell-Reinforced Aeolian Sand Subgrade under Live Traffic. *Applied Sciences (Switzerland)* 13:. <https://doi.org/10.3390/app13020864>
19. Moulay Omar H, Mekerta B, Jarno A, Imanzadeh S, Alem A, Taibi S (2022) Optimization of dune sand-based mixture material for pavement design. *European Journal of Environmental and Civil Engineering* 26:4952–4972. <https://doi.org/10.1080/19648189.2021.1877827>
20. Qureshi MU, Alsaïdi M, Aziz M, Chang I, Rasool AM, Kazmi ZA (2021) Use of reservoir sediments to improve engineering properties of dune sand in oman. *Applied Sciences (Switzerland)* 11:1–13. <https://doi.org/10.3390/app11041620>
21. Smaida A, Cheriet R, Haddadi S, Nechnech A (2022) Valorization of dune sand of Djelfa (Algeria) treated by hydraulic binders in pavement foundations. *Journal of Building Materials and Structures* 9:33–43. <https://doi.org/10.34118/jbms.v9i1.1897>
22. Djeridane M, Zaidi A, Lakhdari MF, Krobba B (2021) Theoretical and Experimental Flexural Behavior of Steel Bars-Reinforced Concrete Beams Strengthened with Cementitious Mortars Based on Dune Sands. *International Journal of Civil Engineering* 19:623–634. <https://doi.org/10.1007/s40999-020-00591-8>
23. Garcia GFN, Lodi PC (2020) Post-cycling Interface Strength Test of Geogrids. *International Journal of Civil Engineering* 18:827–834. <https://doi.org/10.1007/s40999-020-00518-3>

24. Denine S, Della N, Dlawar MR, Sadok F, Canou J, Dupla J-C (3917) Effect of Geotextile Reinforcement on Shear Strength of Sandy Soil: Laboratory Study. *Studia Geotechnica et Mechanica* 38:3–13. <https://doi.org/doi:10.1515/sgem-2016-0026>
25. Denine S, Della N, Muhammed RD, Feia S, Canou J, Dupla J-C (2022) Triaxial behaviour of geotextile reinforced sand. *Geomechanics and Geoengineering* 17:1973–1983. <https://doi.org/10.1080/17486025.2021.1986235>
26. Benessalah I, Arab A, Villard P, Merabet K, Bouferra R (2016) Shear Strength Response of a Geotextile-Reinforced Chlef Sand: A Laboratory Study. *Geotechnical and Geological Engineering* 34:1775–1790. <https://doi.org/10.1007/s10706-016-9988-7>
27. Abdelkader B, Ahmed A, Mostéfa B, Isam S (2016) Laboratory study of geotextiles performance on reinforced sandy soil. *Journal of Earth Science* 27:1060–1070. <https://doi.org/10.1007/s12583-015-0621-0>
28. Feng GY, Wang XY, Zhang DT, Xiao XL, Qian K (2019) Influence of geotextile type on strength and failure behavior of geotextiles reinforced desert sand based on Mohr-Coulomb criterion. *Mater Res Express* 6:. <https://doi.org/10.1088/2053-1591/aae43d>
29. Skuodis Š, Dirgėlienė N, Medzvieckas J (3920) Using Triaxial Tests to Determine the Shearing Strength of Geogrid-Reinforced Sand. *Studia Geotechnica et Mechanica* 42:341–354. <https://doi.org/doi:10.2478/sgem-2020-0005>
30. Jamshidi Chenari R, Ebrahimi Khonachah R, Hosseinpour I, Khajeh A (2020) An Experimental Study for the Cyclic Interface Properties of the EPS–sand Mixtures Reinforced with Geogrid. *International Journal of Civil Engineering* 18:151–159. <https://doi.org/10.1007/s40999-019-00424-3>
31. Markou I (2016) Effect of Grain Shape and Size on the Mechanical Behavior of Reinforced Sand. *Procedia Eng* 143:146–152. <https://doi.org/https://doi.org/10.1016/j.proeng.2016.06.019>
32. Markou IN (2018) A Study on Geotextile—Sand Interface Behavior Based on Direct Shear and Triaxial Compression Tests. *International Journal of Geosynthetics and Ground Engineering* 4:8. <https://doi.org/10.1007/s40891-017-0121-7>
33. Lakkimsetti B, Latha GM (2023) Morphological insights into the liquefaction and post-liquefaction response of sands with geotextile inclusions using drained constant volume simple shear tests. *Geotextiles and Geomembranes* 51:144–164. <https://doi.org/https://doi.org/10.1016/j.geotexmem.2023.06.002>
34. Lal D, Sankar N, Chandrakaran S (2019) Triaxial test on saturated sands reinforced with coir products. *International Journal of Geotechnical Engineering* 13:270–276. <https://doi.org/10.1080/19386362.2017.1343758>
35. Goodarzi S, Shahnazari H (2019) Strength enhancement of geotextile-reinforced carbonate sand. *Geotextiles and Geomembranes* 47:128–139. <https://doi.org/https://doi.org/10.1016/j.geotexmem.2018.12.004>
36. Aldeeky H, Al Hattamleh O, Abu Alfoul B (2016) Effect of Sand Placement Method on the Interface Friction of Sand and Geotextile. *International Journal of Civil Engineering* 14:133–138. <https://doi.org/10.1007/s40999-016-0019-0>

37. Zeng Y, Jiang H, Ding S, Chen J, Wang Y, Zheng J (2021) Analytical and Experimental Investigations on Mechanical Properties of Weak Plane Bedding in Mudstone. *Geofluids* 2021.: <https://doi.org/10.1155/2021/5408701>